

Flame synthesis of $\text{Y}_2\text{O}_3:\text{Eu}$ nanophosphors using ethanol as precursor solvents

Xiao Qin and Yiguang Ju^{a)}

*Department of Mechanical and Aerospace Engineering, Princeton University,
Princeton, New Jersey 08544*

Stefan Bernhard

Department of Chemistry, Princeton University, Princeton, New Jersey 08544

Nan Yao

*Princeton Institute for the Science and Technology of Materials, Princeton University,
Princeton, New Jersey 08544*

(Received 22 April 2005; accepted 28 June 2005)

$\text{Y}_2\text{O}_3:\text{Eu}$ nanophosphors were prepared by flame synthesis using ethanol or water as precursor solutions. The effects of precursor solvents and flame temperature on particle size, morphology, and photoluminescence intensity were investigated. The results showed that flame synthesis using ethanol solution could produce nanoparticles with better homogeneity, smoother surface structure, and stronger photoluminescence intensity than using water. It was found that the concentration quenching limit of the as-prepared nanophosphors from both ethanol and water solution was 18 mol% Eu, which is higher than the reported limit at similar particle size. The x-ray diffraction (XRD) spectra showed that the ethanol precursor solvent produced monoclinic phase $\text{Y}_2\text{O}_3:\text{Eu}$ nanoparticles at a lower flame temperature than previously reported. It was also shown that the particle size could be controlled by varying the precursor concentration and flame temperature.

I. INTRODUCTION

Nanoparticles have become a research focus in terms of both their fundamental and practical importance, especially in the case of luminescent materials.^{1–6} Phosphorous nanoparticles exhibit unique chemical and physical properties compared to their bulk materials. These properties are halfway between molecular and bulk solid state structures.¹ For example, quantum confinement effects, which bring electrons to higher energy levels, can lead to novel optoelectronic properties.⁷ Due to these unique properties, many potential applications in optical, electrical, biological, chemical, and mechanical areas can be developed.^{1,4} Moreover, the emission lifetime, luminescent efficiency, and concentration quenching of the luminescent particles strongly depends on particle size, crystal structure, and hydroxyl residuals.^{2,3}

Among numerous phosphors, europium-doped yttrium oxide ($\text{Y}_2\text{O}_3:\text{Eu}$) has attracted much attention as a good red phosphor that is widely used in optical displays and

lighting applications.⁸ Under ultraviolet (UV) excitation, $\text{Y}_2\text{O}_3:\text{Eu}$ gives a sharp red emission line at 611 nm, and the luminescence efficiency is high because its charge transfer transition is located in the UV range.⁸ Nanoscale $\text{Y}_2\text{O}_3:\text{Eu}$ phosphor has shown significant promise in high-resolution displays (field emission display, flat panel display, thin film electroluminescence panel, etc.) because the quantum efficiency of doped nanocrystals increases as the particle size decreases.^{2,9} Various methods, such as sol-gel techniques,¹⁰ homogeneous precipitation,¹¹ thermal hydrolysis,¹² laser-heated evaporation,¹³ chemical vapor synthesis,¹⁴ microemulsion,^{15,16} spray pyrolysis,¹⁷ combustion synthesis,¹⁸ and flame spray pyrolysis¹⁹ were used to prepare nano-sized $\text{Y}_2\text{O}_3:\text{Eu}$ phosphors.

Flame spray pyrolysis (FSP), also called liquid flame spray (LFS), is a promising particle synthesis method because it can use a wide range of precursors for synthesis of a broad spectrum of functional nanoparticles.^{20–22} The heat released from the combustion of a gaseous or liquid fuel and the precursor itself can provide the high-temperature environment, which is favorable to phosphor synthesis. The flame temperature and particle residence time, which are the most important parameters

^{a)}Address all correspondence to this author.

e-mail: yju@princeton.edu
DOI: 10.1557/JMR.2005.0364

determining the characteristics of the particles,²⁰ can be easily controlled by varying fuel and oxidizer flow rates. Moreover, the particle size can be controlled by varying precursor solution concentration and multi-component particles can also be obtained by adding different salts into the solution.²¹ This technique can also be easily scaled up with high production rates for the manufacture of commercial quantities of nanoparticles.²³

Using FSP method, Kang et al.¹⁹ prepared $Y_2O_3:Eu$ phosphor particles on the order of 1 μm in size and found that the particles had a spherical and dense morphology finer than the particles prepared by general spray pyrolysis. Their as-prepared particles had a monoclinic phase with small impurities of the cubic phase. Tanner and Wong²⁴ synthesized $Y_2O_3:Eu$ nanoparticles using pre-formed sol, spray pyrolysis, and flame spray pyrolysis methods and compared the luminescence properties of the powders prepared by these three methods. Chang et al.²⁵ fabricated cubic nanocrystalline $Y_2O_3:Eu$ phosphors using the FSP method without any post-heat treatments and the x-ray diffraction (XRD) spectra of the as-prepared particles indicated cubic phase with high crystallinity. In flame spray pyrolysis, the precursor composition is a key parameter for achieving the preferred product properties.²¹ As the precursor releases from the droplet, the droplet evaporation, decomposition, and gas phase reaction play important roles in the formation of the final product.

Considering that precursor solution has a significant impact on the flame temperature, nanoparticle size, crystalline structure, and luminescence intensity, it is important to understand how the solvent composition affects the luminescence of nanophosphors. Unfortunately, in the three works mentioned above,^{19,24,25} water was the only precursor solvent. In addition, to the best of our knowledge, there is no report available on the effect of solvent composition on the synthesis of $Y_2O_3:Eu$ phosphorous nanoparticles with flame spray pyrolysis. Moreover, although the effect of flame temperature on the morphology and size distribution of ceramic nanoparticles (SiO_2 , TiO_2 , Al_2O_3 , etc.) was studied in depth,²⁰ its effect on the luminescence of nanophosphors has not been reported.

The objectives of this work are to synthesize $Y_2O_3:Eu$ nanoparticles by the FSP method using both ethanol and water as precursor solvents, and to study the influence of precursor solvents and flame temperature on the morphology and luminescence of the nanophosphors.

II. EXPERIMENTAL

Figure 1 shows the schematic of the flame spray pyrolysis system. The system consisted of a spray generator, a coflow burner, a quartz reactor, particle collection filters, and a vacuum pump. An ultrasonic spray generator operating at 1.7 MHz was used to generate fine spray

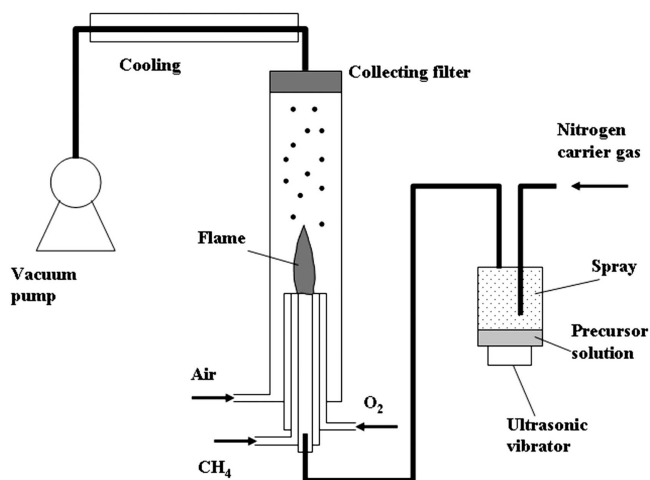


FIG. 1. Schematic illustration of experimental setup.

droplets (mean diameter around 5 μm ²⁶), which were then carried into the flame by nitrogen gas through a central tube of 5.3-mm inner diameter. The flame nozzle consisted of three concentric stainless steel tubes. A methane and oxygen non-premixed flame was used for the flame synthesis. An air coflow was also introduced into the reactor to control the particle residence time. Therefore, by varying the flow rate of methane, oxygen, coflow air, and nitrogen, the flame temperature and particle residence time can be controlled. Temperature measurements along the flame centerline used uncoated 100- μm -diameter R-type thermocouples with a junction bead diameter of $350 \pm 30 \mu\text{m}$ and were corrected for radiation heat losses. The adiabatic flame temperature at equilibrium state was calculated using the CHEMKIN II package,²⁷ where CH_4 , O_2 , N_2 , H_2O , and C_2H_5OH were considered as reactants, and CH_4 , O_2 , N_2 , H_2O , CO_2 , CO , H , OH , O , N , NO , and NO_2 were used as products.

To study the effect of precursor solution on particle formation, ethanol, and water were selected as the solvents. The starting precursor solution was prepared by dissolving a known amount of yttrium and europium nitrate [$Y(NO_3)_3 \cdot 6H_2O$ and $Eu(NO_3)_3 \cdot 6H_2O$, 99.9%, Alfa Aesar, Ward Hill, MA] in distilled water or ethanol. The overall concentration was varied from 0.1 to 0.001 M and the doping concentration of europium varied from 3 to 21 mol% with respect to yttrium.

The particles were collected using a micron glassfiber filter (Whatmann GF/F, Brentford, Middlesex, UK) located 30 cm above the flame. Powder XRD (30 kV and 20 mA, $Cu K_{\alpha}$, Rigaku Miniflex, Tokyo, Japan) was used for crystal phase identification and estimation of the crystalline size. The particle powders were pasted on a quartz glass holder and the scan were conducted in the range of 10° to 60° (2θ). The morphology and size of particles was examined using a field-emission scanning electron microscope (FE-SEM; Philips XL30, Hillsboro,

OR). The photoluminescence spectra of the samples were measured with a Jobin-Yvon Fluorolog-3 fluorometer (Fluorolog-3, HORIBA Jobin-Yvon, Edison, NJ) equipped with a front face detection setup and two double monochromators. The samples were excited at 355 nm with a 150-W Xenon lamp, and a 2-nm slit width was used for both monochromators. The samples were as-prepared powders collected on micron glass fiber filters. All samples were examined at room temperature at 298 K.

III. RESULTS AND DISCUSSION

A. Effect of precursor solvent on particle morphology and size distribution

Figure 2 shows scanning electron microscopy (SEM) photographs of as-prepared $\text{Y}_2\text{O}_3\text{:Eu}$ particles by flame spray pyrolysis using distilled water [Fig. 2(a) and 2(b)] and ethanol [Figs. 2(c) and 2(d)] as precursor solvent at different overall concentrations. The europium doping concentration was 6 mol% with respect to yttrium for all cases. The effect of precursor solution on particle morphology and size can be clearly seen from these images. The particles made from aqueous solution [see Figs. 2(a) and 2(b)] have a hairy structure on the surface and broader size distribution. On the other hand, the particles using ethanol as precursor solution [see Fig. 2(c) and 2(d)] exhibit smoother surface structure and improved

homogeneity in distribution. Regardless of the overall concentration and precursor solvent type, the particles are generally non-aggregated and have a spherical morphology.

Figure 3 shows the size distribution of the particles corresponding to the SEM photographs in Figs. 2(a)–2(d). The distribution has been determined by measuring the diameters of 500 particles from the SEM images. It is seen that particles prepared from ethanol solution exhibit narrower size distributions and smaller average diameters than those from water solution of the same concentration. Table I lists the average particle size, geometric standard deviation calculated from the SEM images at different precursor concentration. The average diameter of the particles varied from 114 to 412 nm when the overall precursor concentration increased from 0.001 to 0.1 M using ethanol as precursor solvent. Table I indicates that the formed particle size can be easily controlled by changing the overall concentration.

The atomized droplet size is related to the surface tension (T) and density (ρ) of the precursor solution, and the ultrasonic nebulizer frequency (f). The average droplet size (D) can be approximately determined by $D = C[T/(\rho f^2)]^{-3}$, where C is a constant. Substituting the properties of water and ethanol into this relation, the average size water droplet is 1.6 times larger than that of ethanol. The smaller ethanol droplet size leads to small final particle size. In Table I, it is seen that the mean diameter of particles from 0.1 M water solution is

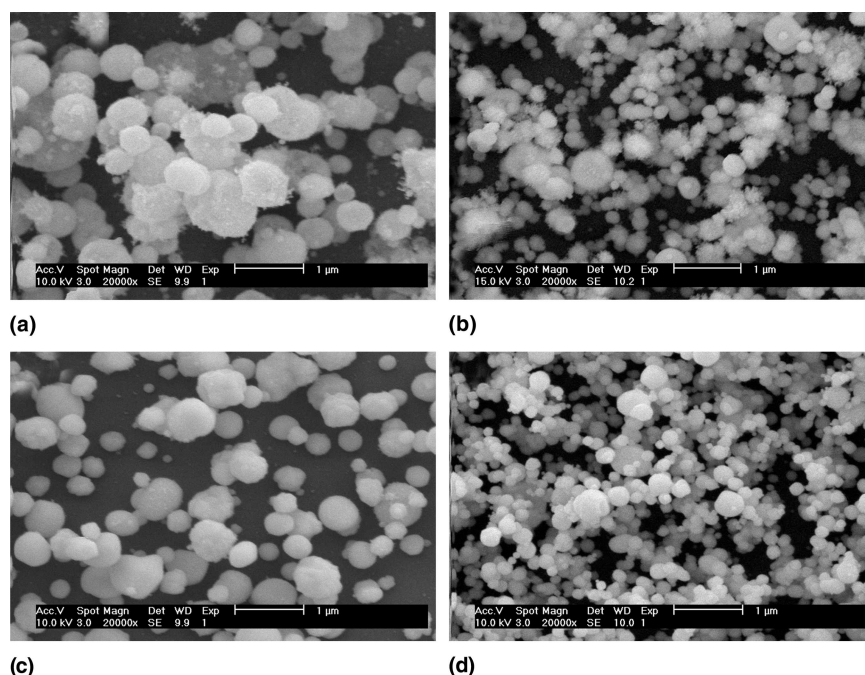


FIG. 2. SEM photographs of $\text{Y}_2\text{O}_3\text{:Eu}$ particles prepared from different precursor solvent and overall concentration: (a) distilled water solution, 0.1 M; (b) distilled water solution, 0.01 M; (c) ethanol solution, 0.1 M; and (d) ethanol solution, 0.01 M. The Eu doping concentration is fixed at 6 mol% with respect to Y for all cases. The scale bar in is 1 μm .

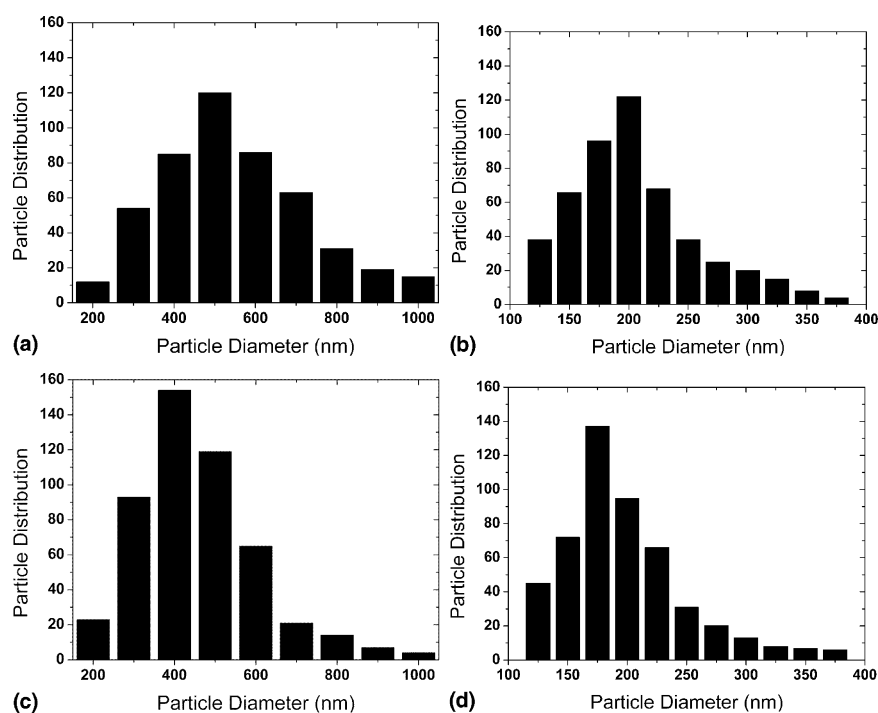


FIG. 3. Size distribution of particles corresponding to the photographs in Figs. 2(a)–2(d) by measuring 500 particles from the SEM images.

512 nm, which is 1.3 times larger than that from 0.1 M ethanol solution (412 nm). The above results demonstrated that the precursor composition has a strong impact on the particle size and morphology and that ethanol solution produces more uniform and well-defined $Y_2O_3:Eu$ nanoparticles than water.

B. Effect of flame temperature

The differences in particle morphology and size distribution when using ethanol and water as precursor solvent arise from the different physical properties between ethanol and water, and the difference of flame temperatures. Ethanol has a lower boiling point and enthalpy of evaporation (78 °C and 838 kJ/kg) than water (100 °C and 2258 kJ/kg). More importantly, ethanol is a fuel that

directly reacts and releases heat to the flame instead of taking away heat from the flame as using water. To investigate the effect of different solutions on the flames, temperature profiles along the centerline for the flames corresponding to Figs. 2(a) and 2(c) were measured by thermocouples and are shown in Fig. 4. During the measurements, methane, oxygen, nitrogen, and coflow air flow rates were kept at 0.169, 1.51, 0.200, and 2.60 l/min, respectively, for the two cases. It should be mentioned that near the core of the methane-oxygen flame (<10 cm), the flame temperature is so high that the thermocouple immediately breaks as it is inserted in the flame; therefore, only data above 10 cm were measured. From Fig. 4, it is seen that the temperature of the flame using ethanol as precursor solvent is consistently 200 K higher than the flame using water, although the adiabatic flame temperature from CHEMKIN calculation is the same of 2128 K

TABLE I. Average diameter, geometric standard deviation (by measuring 500 particles from the SEM images) of the as-prepared particles, and flame temperature with different overall precursor concentration and fixed Eu doping concentration of 6 mol% with respect to Y.

Case	Precursor concentration (M)	Precursor type	Average diameter (nm)	Geometric standard deviation	Flame temperature ^a (K)
1 [Fig. 2(a)]	0.1	Water	535	1.20	1720
2 [Fig. 2(b)]	0.01	Water	192	1.31	1720
3 [Fig. 2(c)]	0.1	Ethanol	412	1.14	2020
4 [Fig. 2(d)]	0.01	Ethanol	198	1.10	2020
5	0.001	Ethanol	114	1.07	2020

^aAt centerline location of 10 cm above the burner exit.

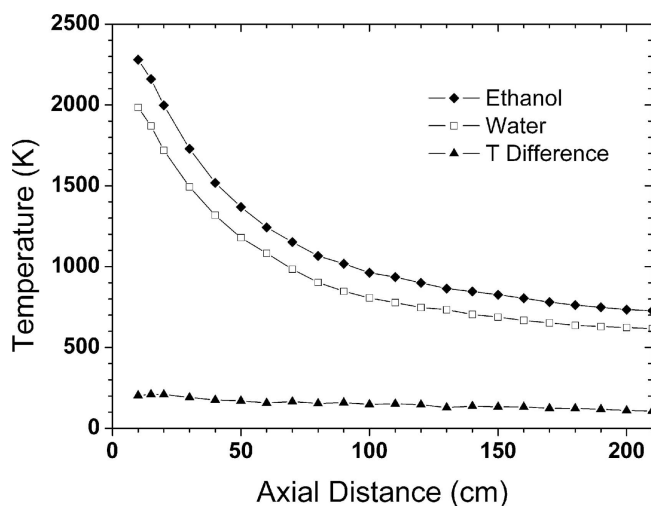


FIG. 4. Temperature distribution along the centerline for the flames corresponding to SEM images in Figs. 2(a) and 2(c).

for these two flames. Here, air coflow was not considered and the flow rate of ethanol or water was about 8.67×10^{-2} ml/min and showed little effect (less than 1 K) in the equilibrium temperature calculation.

Generally, in flame spray pyrolysis higher flame temperature increases particle sintering and agglomerating,²⁰ which is not the case in our observation from Figs. 2(a) and 2(c) for different precursor solutions. From simplified analysis, the D -square law that describes a single droplet evaporation can be expressed as $D^2(t) = D_0^2 - Kt$, where D is the droplet diameter at time t and D_0 is the initial droplet diameter. The evaporation constant $K = 8\lambda_g \ln(1 + B)/(\rho_l c_{pg})$, where λ_g is the thermal conductivity of the gas surrounding the droplet, ρ_l the liquid density, and c_{pg} the heat capacity of the gas. B is the Spalding number, $B = c_{pg}(T_\infty - T_d)/h_{fg}$, where T_∞ is the gas temperature, T_d the droplet temperature that equals its boiling temperature, and h_{fg} the latent heat of vaporization. The droplet lifetime t_d can be determined as $t_d = D_0^2/K$. Assuming that the surrounding gas is oxygen (which is about 10 times more than methane) and the gas temperature T_∞ is 1200 K, then $\lambda_g = 0.0819$ W/m K, $c_{pg} = 1115$ J/kg K. For water, when $T_d = 373$ K, $h_{fg} = 2258$ kJ/kg, the lifetime of a water droplet of initial diameter of $5.0 \mu\text{m}$ is $66.2 \mu\text{s}$. The lifetime of an ethanol droplet of the same size is $24.1 \mu\text{s}$. Suppose that the thickness of the preheat zone is 0.5 mm, and the droplet velocity is 50 cm/s; then the residence time that the droplet in the preheat zone is $1000 \mu\text{s}$, which is much longer than the droplet lifetime. Therefore, the droplet is totally vaporized before it reaches the reaction zone (flame). This suggests that the initial droplet size and precursor concentration are the dominant factors that determine the final particle size. This explains that even though the temperature is higher in the flame using ethanol solution,

the smaller ethanol droplets evaporate faster when passing the preheat zone and produces smaller final particles. Limaye and Helble²⁸ observed similar effect of precursor and solvents on the morphology of zirconium nanoparticles produced by combustion aerosol synthesis.

On the other hand, we kept the oxygen, nitrogen, and air flow rates at 1.51 , 0.213 , and 3.18 l/min, respectively, and adjusted the methane flow rate (0.115 , 0.169 , and 0.223 l/min) for flame using 0.01 M ethanol solution, then three flames with adiabatic flame temperature of 1695 , 2135 , and 2431 K were obtained. As listed in Table II, the temperature at the centerline location of 20 cm above the burner exit is 1539 , 1892 , and 2130 K, respectively. The average particle sizes are 185 , 198 , and 214 nm. The flame length for case 3 is about 10 cm longer than in case 1. At higher flame temperatures the sintering and coagulation rates increase and enhance the formation of larger particles. The longer flame length increases the residence time of particles and gives more time for the particles to grow. This is in agreement with the report of Mädler et al.,²² who found an increase of silica particle sizes with higher adiabatic flame temperature.

C. Effect of precursor solvent on crystal structure

The powder XRD patterns of the $Y_2O_3:Eu$ nanoparticles prepared by using water/ethanol as precursor solvent are shown in Fig. 5. For particles from water solution, the XRD spectrum [Fig. 5(a)] indicates a cubic structure of $Y_2O_3:Eu$ with the peaks corresponding to the (211), (222), (400), (411), (420), (413), (440), (611), and (622) planes when compared with International Center for Diffraction Data (ICDD) Card No. 25-1011³² of cubic $(Y_{0.95}Eu_{0.05})_2O_3$ [see Fig. 5(b)]. No peak of any other phase was detected. The average crystallite size of the particles can be calculated by Scherrer equation: $D = 0.89\lambda/(B)\theta$, where λ ($= 0.1540598$ nm), θ , and B are the wavelength of the x-ray, the diffraction angle, and the full width at half-maximum (FWHM) of the XRD peaks (corresponding to 2θ), respectively; and 0.89 is a constant for spherical particles. The crystallite sizes for the

TABLE II. Average diameter, geometric standard deviation (by measuring 500 particles from the SEM images) of the as-prepared particles at different flame conditions for 0.01 M ethanol solution with 6 mol% Eu doping concentration.

Case	Flame temperature ^a (K)	Adiabatic flame temperature (K)	Average diameter (nm)	Geometric standard deviation
6	1539	1695	185	1.07
7	1892	2135	198	1.10
8	2130	2431	214	1.09

^aAt centerline location of 20 cm above the burner exit.

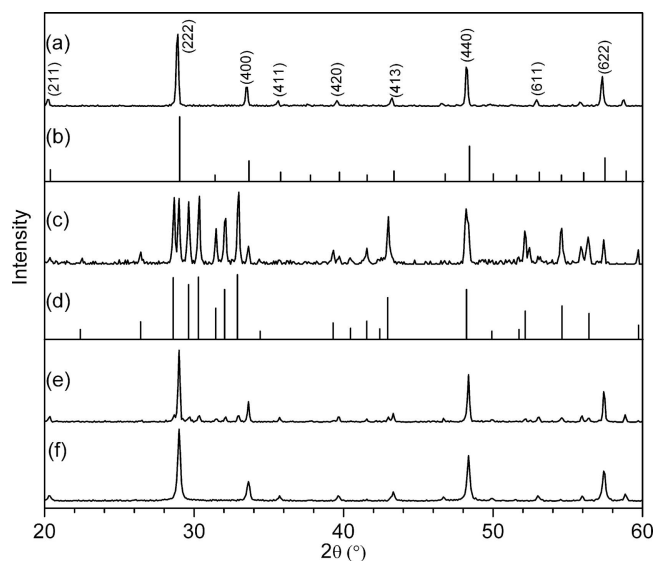


FIG. 5. XRD spectra of (a) as-prepared $Y_2O_3:Eu$ particles from water solution, (b) ICDD No. 25-1011³² (cubic $Y_2O_3:Eu$), (c) as-prepared $Y_2O_3:Eu$ particles from ethanol solution, (d) ICDD No. 44-0399³³ (monoclinic Y_2O_3), (e) as-prepared $Y_2O_3:Eu$ particles from water solution at higher flame temperature, and (f) $Y_2O_3:Eu$ particles from ethanol solution after 2 h annealing at 1200 °C.

cases in Figs. 5(a), 5(c), 5(e), and 5(f) are 41.4, 43.6, 58.4, and 56.1 nm, respectively.

The XRD spectrum of the as-prepared particles from ethanol solution [see Fig. 5(c)] shows significant difference from that in Fig. 5(a). In addition to the peaks from the cubic phase, other peaks are supposed to come from monoclinic phase of $Y_2O_3:Eu$. Since no data were available in the PDF database of ICDD for monoclinic $Y_2O_3:Eu$, the additional peaks were compared with monoclinic Y_2O_3 of ICDD Card No. 44-0399³³ [Fig. 5(d)] and the peaks from monoclinic phase can be clearly identified. The pattern in Fig. 5(c) is similar to the XRD spectra of Okumura et al.²⁹ who prepared monoclinic phase $Y_2O_3:Eu$ particles by inductively coupled thermal plasma. Kang et al.¹⁹ and Chang et al.²⁵ reported that a low adiabatic temperature flame (<2864 K) results in cubic phase $Y_2O_3:Eu$ while a high-temperature flame produces particles with monoclinic phase in their flame synthesis using distilled water as solvent. However, the adiabatic flame temperature in our case of Fig. 5(c) is 2128 K, which is much lower than 2873 K, but monoclinic phase was obtained. Therefore, the different crystal structure of the particles using water and ethanol as solvent cannot only be explained by the flame temperature difference; the effect of solvent itself also contributes. By increasing methane flow rate and raising adiabatic flame temperature to 2430 K in the flame using water solution, monoclinic phase $Y_2O_3:Eu$ particles were observed, as can be seen from XRD spectrum in Fig. 5(e). $Y_2O_3:Eu$ with monoclinic phase has low thermal stability. By annealing the particles prepared from ethanol solution at

1200 °C for 2 h, the monoclinic phase changed into cubic phase completely [see Fig. 5(f)].

D. Effect of precursor solvent on photoluminescence

Figure 6 shows the photoluminescence spectra of $Y_2O_3:Eu$ nanoparticles excited by UV light at the wavelength of 355 nm. The spectrum of the as-prepared particles prepared from water solution shows a typical $Y_2O_3:Eu^{3+}$ emission spectrum, which is described by the well known $^5D_0 \rightarrow ^7F_J$ ($J = 0, 1, 2 \dots$) line emissions of the Eu^{3+} ions. The strongest emission at 611 nm is a hypersensitive forced electric-dipole emission from $^5D_0 \rightarrow ^7F_2$ transition, and the peaks around 600 nm correspond to the $^5D_0 \rightarrow ^7F_1$ transition, which is a magnetic-dipole emission. However, the photoluminescence spectra of the particles obtained from ethanol solution shows a double peak at 615 and 624 nm, respectively. These two peaks are caused by the $^5D_0 \rightarrow ^7F_2$ transition from

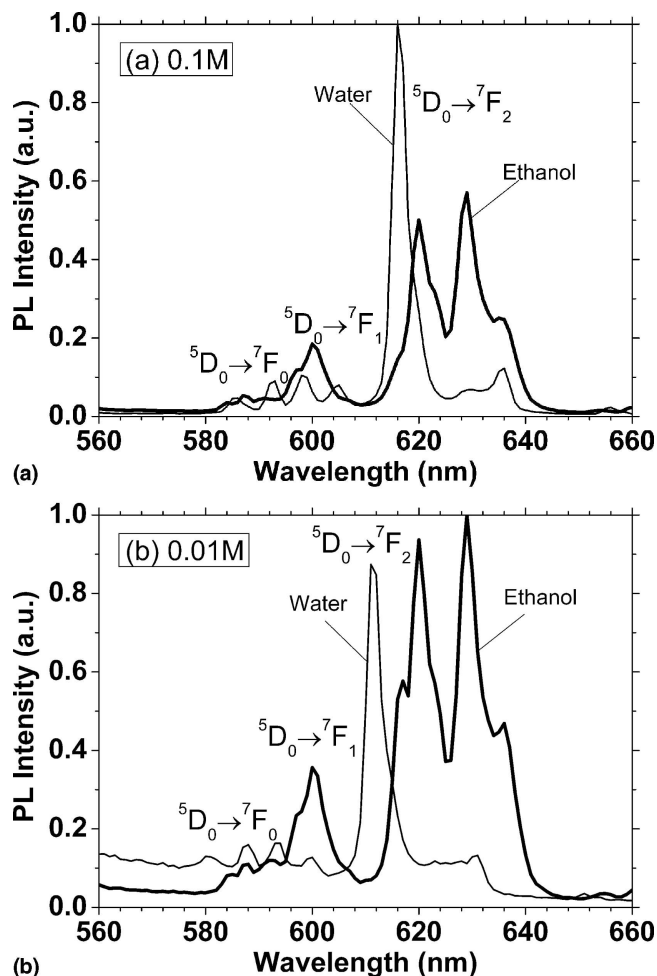


FIG. 6. Photoluminescence spectra of as-prepared $Y_2O_3:Eu$ nanoparticles from water and ethanol solution of different overall precursor concentration: (a) 0.1 M and (b) 0.01 M. The Eu doping concentration is 6 mol% with respect to Y. The mean particle size is listed in Table I.

the monoclinic $Y_2O_3:Eu$. By annealing the particle from ethanol solution at 1200 °C for 2 h transformed the monoclinic phase into cubic phase and resulted in single peak PL spectra (not shown here). Comparing Figs. 6(a) and 6(b), the overall concentration of the precursor show little effect on the shape of PL spectra, but the relative intensity changes for the two types of particles. The integral PL intensity from particles using ethanol is 30% and 90%, respectively, higher than that of particles using water as solvent for 0.1 M [Fig. 6(a)] and 0.01 M [Fig. 6(b)] solution. This is because that higher flame temperature enhances photoluminescence intensity, which can be illustrated in Fig. 7.

Figure 7 shows the influence of flame temperature on photoluminescence intensity of particles prepared from ethanol solution. The brightness of the as-prepared particles was strongly affected by flame temperatures. As the flame temperature increases from 1539 to 2130 K (measured at 20 cm above the burner exit), the integral PL intensity increases more than 250%. Also, the peak intensity at 611 nm increases but decreases at 624 nm. At high flame temperatures, the crystallinity of the particles becomes higher, and the brightness of the as-prepared particles increases. Similar observations were reported when increasing furnace temperature in their combustion synthesis of luminescent oxides by Shea et al.³⁰

E. Concentration quenching limit

It is known that when the activator concentration (Eu^{3+}) increases to a limit level, luminescence begins to quench. The pairing and aggregation of activator atoms at high concentration may change a fraction of the activators into quenchers and induce the quenching effect. The migration of excitation by resonant energy transfer

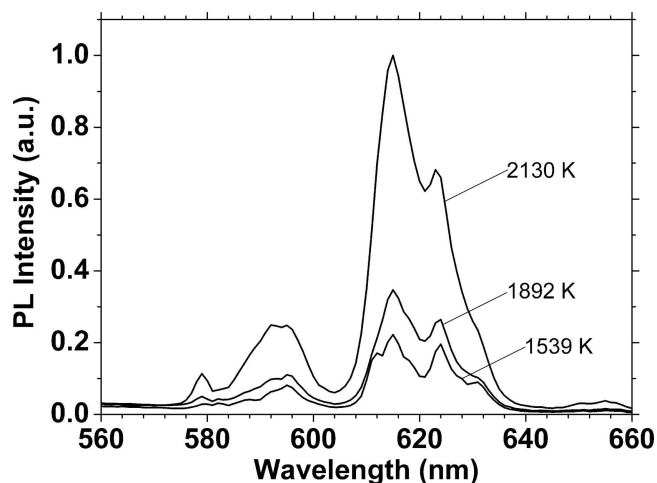


FIG. 7. Effect of flame temperature on photoluminescence intensity for as-prepared $Y_2O_3:Eu$ particles using ethanol as precursor solvent. The temperature in the legend represents values at 20 cm above the burner exit. The mean particle size is listed in Table II.

between Eu^{3+} activators can also incur quenching.¹⁵ In bulk $Y_2O_3:Eu$ phosphors, the concentration quenching occurs around 6 mol% Eu with respect to Y.^{12,31} Figure 8 shows the effect of Eu doping concentration on the photoluminescence intensity of the as-prepared $Y_2O_3:Eu$ nanoparticles using ethanol as precursor solvent at fixed 0.1 M overall precursor concentration. Here, the particle size is constant as can be confirmed from SEM images, and europium concentration alteration had little influence on the particle size. Different from the reported 6 mol% Eu for bulk materials, the quenching concentration is 18 mol% for particles prepared using both ethanol and water (not shown here) solutions in the present study. Table III lists the reported quenching concentrations by different synthesis methods in the literature. The quenching concentration varies from 4% to 18% and is different even for the same method at similar crystalline size. Tao et al.¹⁸ reported a value of 14% and argued that the decrease of the energy transfer due to the interface effects

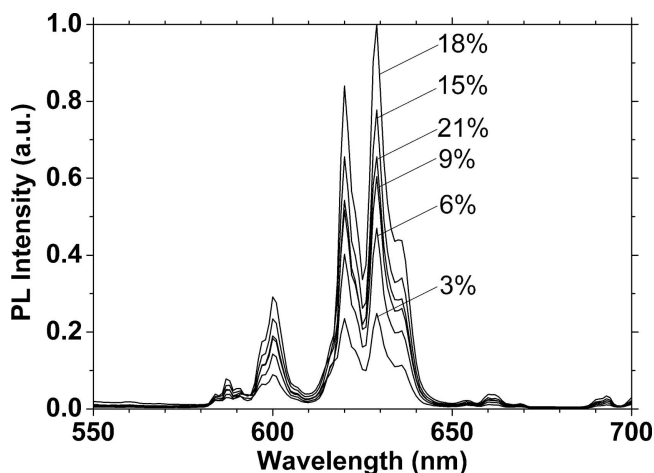


FIG. 8. Photoluminescence spectra of $Y_2O_3:Eu$ nanoparticles at different doping concentration (Eu mol% with respect to Y). The overall precursor concentration is fixed at 0.1 M.

TABLE III. Quenching concentration and corresponding crystalline size reported in the literature.

Authors	Synthesis method	Quenching concentration (mol%)	Crystalline size (nm)
He et al. ¹¹	Precipitation	4%	33
Pang et al. ¹⁶	Microemulsion	6%	25
Kang et al. ¹⁷	Spray pyrolysis	6%	770
Sharma et al. ¹²	Hydrolysis	6%	...
Zhang et al. ³⁰	Combustion synthesis	6%	3000
Huang et al. ¹⁵	Microemulsion	10%	18
Chang et al. ²⁵	Flame spray pyrolysis	12%	40
Zhang et al. ³⁰	Combustion synthesis	13%	40
Tao et al. ¹⁸	Combustion synthesis	14%	70
Zhang et al. ³⁰	Combustion synthesis	18%	5
This work	Flame spray pyrolysis	18%	50

of the nanoparticles increases the quenching concentration. Zhang et al.³¹ reported that the quenching concentration was 6, 13, and 18 mol% when the crystallite size was 3 μm , 40 nm, and 5 nm, respectively. Although our 18% quenching limit is in agreement with the 5 nm result of Zhang et al.,³¹ the mean crystalline size in Fig. 8 is about 50 nm, and the mean particle size is around 410 nm, which is larger than that of Zhang et al.³¹ This implies that the increase of quenching concentration limit is not only determined by the decrease of crystalline (particle) size, but also is affected by other factors, such as surface area, etc.

IV. CONCLUSIONS

Europium-doped yttrium oxide ($Y_2O_3:Eu$) nanoscale phosphors were successfully synthesized by flame spray pyrolysis using ethanol as precursor solvent. The results showed that the changes of precursor solvent and flame temperature have significant impact on particle size, morphology, and photoluminescence intensity. SEM photographs showed that using ethanol solutions particles with better homogeneity and smoother surface structure were produced than using water solutions. It was also demonstrated that the particle size could be well controlled by varying the precursor concentration, flame temperature and particle residence time. Moreover, XRD spectra showed that monoclinic phase of $Y_2O_3:Eu$ nanoparticles were obtained by using ethanol as precursor solvent at lower flame temperatures than previously reported. All as-prepared particles showed red emission spectra under the UV excitation. The nanophosphor photoluminescence intensity from ethanol solution was 90% stronger than those from water solution. The concentration quenching limit was found to be 18 mol% Eu, which is higher than the reported quenching limit at the same particle size. The Eu-doped yttria nanophosphors synthesized here may be of potential applications in high resolution displays and as biomedical markers.

ACKNOWLEDGMENT

Y. Ju would like to acknowledge support from National Science Foundation via Grant No. DMR-0303947.

REFERENCES

1. F.E. Krus, H. Fissan, and A. Peled: Synthesis of nanoparticles in the gas phase for electronic, optical and magnetic applications—A review. *J. Aerosol Sci.* **29**, 511 (1998).
2. R.N. Bhargava, D. Gallagher, X. Hong, and A. Nurmikko: Optical properties of manganese-doped nanocrystals of ZnS. *Phys. Rev. Lett.* **72**, 416 (1994).
3. C. Suryanarayana: Nanocrystalline materials. *Int. Mater. Rev.* **40**, 41 (1995).
4. R.N. Bhargava: Doped nanocrystalline materials—Physics and applications. *J. Lumin.* **70**, 85 (1996).
5. R.P. Rao: Preparation and characterization of fine-grain yttrium-based phosphors by sol-gel process. *J. Electrochem. Soc.* **143**, 189 (1996).
6. R. Bazzi, M.A. Flores, C. Louis, K. Lebbou, W. Zhang, C. Dujardin, X. Roux, B. Mercier, G. Ledoux, E. Bernstein, P. Perriat, and O. Tillement: Synthesis and properties of europium-based phosphors on the nanometer scale: Eu_2O_3 , $Gd_2O_3:Eu$, and $Y_2O_3:Eu$. *J. Colloid Int. Sci.* **273**, 191 (2004).
7. A.D. Yoffe: Low-dimensional systems: Quantum-size effects and electronic properties of semiconductor microcrystallites (zero-dimensional systems) and some quasi-two-dimensional systems. *Adv. Phys.* **42**, 173 (1993).
8. G. Blasse and B.C. Grabmaier: *Luminescent Materials* (Springer, Berlin, Germany, 1994).
9. E.T. Goldburt, B. Kulkarni, R. Bhargava, J. Taylor, and M. Libera: Size dependent efficiency in Tb doped Y_2O_3 nanocrystalline phosphor. *J. Lumin.* **190**, 72 (1997).
10. C.N.R. Rao: Chemical synthesis of solid inorganic materials. *Mater. Sci. Eng. B* **18**, 1 (1993).
11. C. He, Y. Guan, L. Yao, W. Cai, X. Li, and Z. Yao: Synthesis and photoluminescence of nano- $Y_2O_3:Eu^{3+}$ phosphors. *Mater. Res. Bull.* **38**, 973 (2003).
12. P.K. Sharma, M.H. Jilavi, R. Nass, and H. Schmidt: Tailoring the particle size from μm \rightarrow nm scale by using a surface modifier and their size effect on the fluorescence properties of europium doped yttria. *J. Lumin.* **82**, 187 (1999).
13. H. Eilers and B.M. Tissue: Laser spectroscopy of nanocrystalline Eu_2O_3 and $Eu^{3+}:Y_2O_3$. *Chem. Phys. Lett.* **251**, 74 (1996).
14. A. Konrad, T. Fries, A. Gahn, F. Kummer, U. Herr, R. Tidecks, and K. Samwer: Chemical vapor synthesis and luminescence properties of nanocrystalline cubic $Y_2O_3:Eu$. *J. Appl. Phys.* **86**, 3129 (1999).
15. H. Huang, G.Q. Xu, W.S. Chin, L.M. Gan, and C.H. Chew: Synthesis and characterization of $Eu:Y_2O_3$ nanoparticles. *Nanotechnology* **12**, 318 (2002).
16. Q. Pang, J. Shi, Y. Liu, D. Xing, M. Gong, and N. Xu: A novel approach for preparation of $Y_2O_3:Eu^{3+}$ nanoparticles by microemulsion-microwave heating. *Mater. Sci. Eng. B* **103**, 57 (2003).
17. Y.C. Kang, S.B. Park, I.W. Lenggoro, and K. Okuyama: Preparation of nonaggregated $Y_2O_3:Eu$ phosphor particles by spray pyrolysis method. *J. Mater. Res.* **14**, 2611 (1999).
18. Y. Tao, G.W. Zhao, W.P. Zhang, and S.D. Xia: Combustion synthesis and photoluminescence of nanocrystalline $Y_2O_3:Eu$ phosphors. *Mater. Res. Bull.* **32**, 501 (1997).
19. Y.C. Kang, D.J. Seo, S.B. Park, and H.D. Park: Morphological and optical characteristics of $Y_2O_3:Eu$ phosphor particles prepared by flame spray pyrolysis. *Jpn. J. Appl. Phys.* **40**, 4083 (2001).
20. S.E. Pratsinis: Flame aerosol synthesis of ceramic powders. *Prog. Energy Combust. Sci.* **24**, 197 (1998).
21. H.K. Kammler, L. Madler, and S.E. Pratsinis: Flame synthesis of nanoparticles. *Chem. Eng. Technol.* **24**, 6 (2001).
22. L. Mädler, H.K. Kammler, R. Mueller, and S.E. Pratsinis: Controlled synthesis of nanostructured particles by flame spray pyrolysis. *J. Aerosol Sci.* **33**, 369 (2002).
23. N.G. Glumac, Y.J. Chen, G. Skandan, and B. Kear: Scalable high-rate production of non-agglomerated nanopowders in low pressure flames. *Mater. Lett.* **34**, 148 (1998).
24. P.A. Tanner and K.L. Wong: Synthesis and spectroscopy of lanthanide ion-doped Y_2O_3 . *J. Phys. Chem. B* **108**, 136 (2004).

25. H. Chang, I.W. Lenggoro, K. Okuyama, and T.O. Kim: Continuous single-step fabrication of nonaggregated, size-controlled and cubic nanocrystalline $Y_2O_3:Eu^{3+}$ phosphors using flame spray pyrolysis. *Jpn. J. Appl. Phys.* **43**, 3535 (2004).
26. I.W. Lenggoro, T. Hata, and F. Iskandar: An experimental and modeling investigation of particle production by spray pyrolysis using a laminar flow aerosol reactor. *J. Mater. Res.* **15**, 733 (2000).
27. R.J. Kee, J.F. Grcar, M.D. Smooke, and J.A. Miller: CHEMKIN-II: A fortan chemical kinetics package for the analysis of gas-phase chemical and plasma kinetics. SANDIA report SAND85-8240, (Sandia National Laboratories, Albuquerque, NM, 1994).
28. A.U. Limaye and J.J. Helble: Effect of precursor and solvent on morphology of zirconia nanoparticles produced by combustion aerosol synthesis. *J. Am. Ceram. Soc.* **86**, 273 (2003).
29. M. Okumura, M. Tamatani, A.K. Albessard, and N. Matsuda: Luminescence properties of rare earth io-doped monoclinic yttrium sesquioxide. *Jpn. J. Appl. Phys.* **36**, 6411 (1997).
30. L.E. Shea, J. McKittrick, O.A. Lopez, and E. Sluzky: Synthesis of red-emitting, small particle size luminescent oxides using an optimized combustion process. *J. Am. Ceram. Soc.* **79**, 3257 (1996).
31. W-W. Zhang, W-P. Zhang, P-B. Xie, M.Y.H-T. Chen, L. Jing, Y-S. Zhang, L-R. Lou, and S-D. Xia: Optical properties of nanocrystalline $Y_2O_3:Eu$ depending on its odd structure. *J. Colloid Interface. Sci.* **262**, 588 (2003).
32. The International Centre for Diffraction Data, <http://www.icdd.com>, PDF#25-1011.
33. The International Centre for Diffraction Data, <http://www.icdd.com>, PDF #44-0399.